

Article

# Phase Stability and Magnetic Properties of $Mn_3Z$ ( $Z = Al, Ga, In, Tl, Ge, Sn, Pb$ ) Heusler Alloys

Haopeng Zhang <sup>1</sup>, Wenbin Liu <sup>1</sup>, Tingting Lin <sup>1,2</sup>, Wenhong Wang <sup>3</sup> and Guodong Liu <sup>1,\*</sup>

<sup>1</sup> School of Physics and Electronic Engineering, Chongqing Normal University, Chongqing 400044, China; hpzhang0201@126.com (H.Z.); wbliu1106@126.com (W.L.); tlin@tmm.tu-darmstadt.de (T.L.)

<sup>2</sup> Institute of Materials Science, Technische Universität Darmstadt, 64287 Darmstadt, Germany

<sup>3</sup> Beijing National Laboratory for Condensed Matter Physics, Institute of Physics, Chinese Academy of Sciences, Beijing 100080, China; wenhong.wang@iphy.ac.cn

\* Correspondence: gdliu1978@126.com

Received: 20 November 2018; Accepted: 5 December 2018; Published: 7 March 2019



**Abstract:** The structural stability and magnetic properties of the cubic and tetragonal phases of  $Mn_3Z$  ( $Z = Ga, In, Tl, Ge, Sn, Pb$ ) Heusler alloys are studied by using first-principles calculations. It is found that with the increasing of the atomic radius of Z atom, the more stable phase varies from the cubic to the tetragonal structure. With increasing tetragonal distortion, the magnetic moments of Mn (A/C and B) atoms change in a regular way, which can be traced back to the change of the relative distance and the covalent hybridization between the atoms.

**Keywords:** phase stability; magnetic properties; covalent hybridization

## 1. Introduction

Tetragonal Heusler compounds have been receiving huge attention in recent years due to their potential applications in spintronic [1–5] and magnetoelectronic devices [6–9], such as ultrahigh density spintronic devices [9–13], spin-transfer torque (STT) [9–16] and permanent hard magnets [17,18]. Among the tetragonal Heusler compounds,  $Mn_3$ -based Heusler compounds exhibit very interesting properties. The previous theoretical and experimental studies [4,16,19–22] show that the tetragonal ( $DO_{22}$ ) phase of  $Mn_3Ga$  compound is ferrimagnetic at room temperature and shows a unique combination of magnetic and electronic properties, including low magnetization, high uniaxial anisotropy, high spin polarization, and high Curie temperature. Because of these interesting properties, this material is believed to have potential for nanometer-sized spin transfer torque (STT) -based nonvolatile memories [4,16,23]. The first-principles calculations reveal that  $Mn_3Z$  ( $Z = Ga, Sn$  and  $Ge$ ) type Heusler compounds can have three different structural phases, where each phase exhibits different magnetic properties [24]. There are also some other reports about the phase stability and the magnetic properties for these systems [25–28], but the relation between the phase stability and the magnetic properties of  $Mn_3Z$  tetragonal Heusler alloys has not been investigated in detail.

In this paper, the relation between the phase stability, magnetic properties, the covalent hybridization effect, and the relative position between atoms of  $Mn_3Z$  ( $Z = Al, Ga, In, Tl, Si, Ge, Sn, Pb$ ) Heusler alloys has been investigated by using the first-principles calculations. It is found that the atomic radius of Z atoms and the level of distortion have great effects on the degree of the covalent hybridization between atoms in  $Mn_3Z$  system, which plays an important role in the phase stability and the magnetic properties of  $Mn_3Z$  Heusler compounds.

## 2. Calculation Details

The calculations of total energy, electronic structure, and magnetic moments were performed by the Cambridge Serial Total Energy Package (CASTEP) code based on the pseudopotential method with a plane-wave basis set [29]. The exchange and correlation effects were treated using the local density approximation (LDA) [30]. The plane wave basis set cut-off was 500 eV for all of the cases, and 182 k-points were employed in the irreducible Brillouin zone. The convergence tolerance for the calculations was selected as the difference in the total energy within the  $1 \times 10^{-6}$  eV/atom. These parameters ensure good convergences for the total energy.

## 3. Results and Discussion

Heusler alloys crystallize in a highly-ordered cubic structure, and have a stoichiometric composition of  $X_2YZ$ , where X and Y are transition-metal elements, and Z is a main group element. Generally, the Heusler structure can be considered as four interpenetrating f.c.c lattices along the space diagonal, in which the transition metal atoms occupy the A (0, 0, 0), B (0.25, 0.25, 0.25) and C (0.5, 0.5, 0.5) Wyckoff positions, respectively. The main group element occupies the D (0.75, 0.75, 0.75) position. The tetragonal Heusler alloys can be considered as tetragonal distortions of the cubic phase along the z direction, and the c/a ratio can be used to quantify the amount of tetragonal distortion [9,31,32]. For tetragonal  $Mn_3Z$  (Z = Al, Ga, In, Tl, Si, Ge, Sn, Pb) alloys, the Mn(A), Mn(B), Mn(C) and Z atoms occupy the (0, 0, 0), (0.25, 0.25, 0.25), (0.5, 0.5, 0.5) and (0.75, 0.75, 0.75) Wyckoff positions, respectively.

As a typical example, we first present the results of  $Mn_3Ga$  alloy. Figure 1 shows the total energy as a function of c/a ( $\Delta E_{total-c/a}$  curve) for  $Mn_3Ga$  alloy. The total energy of the cubic phase is set as the zero point. The lattice constant of the cubic phase is obtained by minimizing the total energy and is 5.66 Å. The unit cell volume is the same as that of cubic phase, and is fixed when the tetragonal distortion is considered. From Figure 1, it can be seen that there are two local energy minima on the  $\Delta E_{total-c/a}$  curve, i.e., a shallow one is at c/a = 1.35 and a deeper one at c/a = 1. The latter is energetically favorable. Between the two energy minima, there is an energy barrier at c/a = 1.15. The lower and upper insets show the corresponding crystal structures, band structures, and densities of states (DOS) for the cubic (c/a = 1) and distorted (c/a = 1.35) cases. From the band structures, we can see that the cubic phase (c/a = 1) of  $Mn_3Ga$  is close to the half-metal, with a high degree of spin polarization. But in the tetragonal phase (c/a = 1.35), the band structure is completely different from the cubic one, and it can also be seen that the spin polarization declines rapidly at the Fermi level from the density of states patterns. This is mainly due to the fact that cubic symmetry is reduced after the tetragonal distortion.

Comparing the work reported by Delin Zhang et al. [31] with that by Claudia Felser et al. [33], it can be noted that the difference of volume can have a large impact on the  $\Delta E_{total-c/a}$  curves. Therefore, we performed a series of investigations on the tetragonal distortion with different volumes to further understand the relation between the volume and the  $\Delta E_{total-c/a}$  curves for  $Mn_3Ga$  alloy. In Figure 2a, we show the  $\Delta E_{total-c/a}$  curves of  $Mn_3Ga$  alloy with different volumes ( $v = 17.0 \text{ nm}^3, 18.0 \text{ nm}^3, 19.0 \text{ nm}^3, 20.0 \text{ nm}^3, 21.0 \text{ nm}^3, 22.0 \text{ nm}^3$ ), which correspond to the different lattice constants in the cubic phase. It can be seen that the shape of the  $\Delta E_{total-c/a}$  curves varies with the change of the volume. There are two local energy minima in the  $\Delta E_{total-c/a}$  curves for all the  $Mn_3Ga$  alloys with different volumes. For  $V = 17.0 \text{ nm}^3$  and  $18.0 \text{ nm}^3$ , the total energy of cubic phase is lower than that of the tetragonal phase, which indicates that the cubic phase is more stable than the tetragonal phase. As the volume expands to higher level than  $19.0 \text{ nm}^3$ , the total energy of the tetragonal phase becomes lower than the cubic phase. At same time, the energy barrier from the cubic phase to the tetragonal phase gradually decreases with the increasing volume, and finally, disappears at  $V = 21.0 \text{ nm}^3$ . This indicates that the tetragonal phase becomes a more stable phase with the expanding volume, and it becomes easier to transform from the cubic phase to the tetragonal phase. So, from the  $\Delta E_{total-c/a}$  curves with different volume of  $Mn_3Ga$ , it is clear that a very small change of the volume can lead to a great change of the shape of the  $\Delta E_{total-c/a}$  curves. In other word, the phase stability of  $Mn_3Ga$  Heusler alloys

is very sensitive to the change of the volume. For the  $Mn_3Ga$  systems, we can adjust the volume to achieve the alloys with different structures as well as possible martensitic transformations.

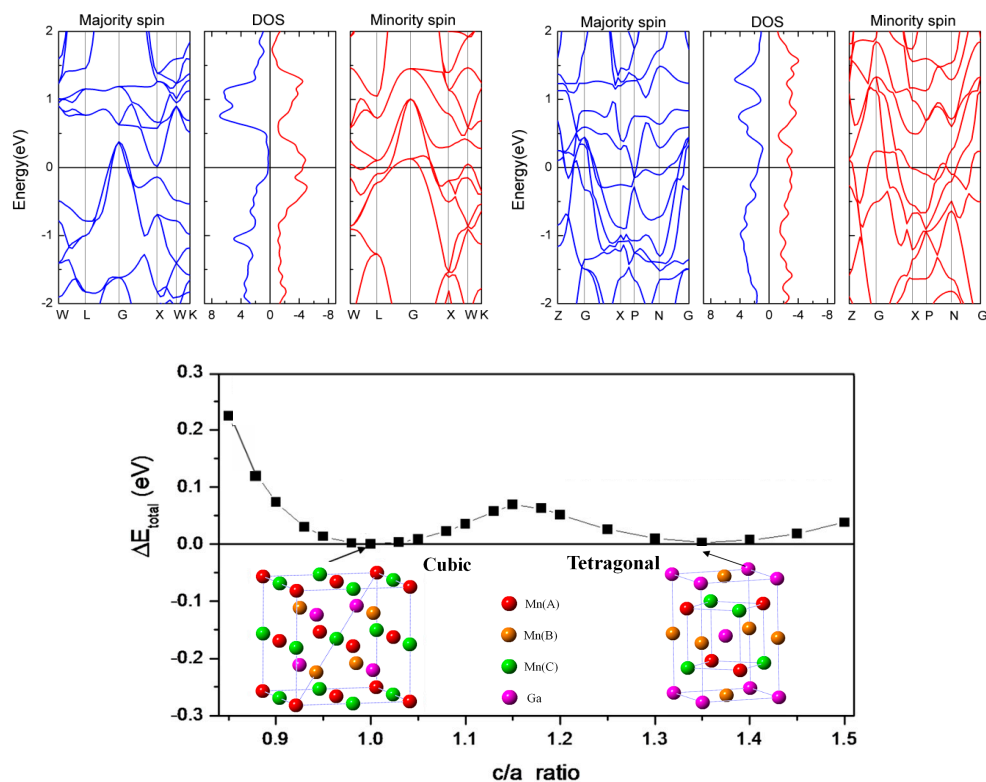


**Figure 1.** Total energy difference (per formula unit) relative to the cubic phase as a function of  $c/a$  for  $Mn_3Ga$  alloy ( $\Delta E_{total} = E_{total}(c/a) - E_{total}(c/a = 1)$ ). The lower insets show the corresponding crystal structures and the upper insets show the band structures and densities of states for the cubic ( $c/a = 1$ ) and distorted ( $c/a = 1.35$ ) phases.

A good way to adjust the volume is to dope similar elements into the matrix. Therefore, next, we extend the research scope to all the other  $Mn_3Z$  ( $Z = Al, In, Tl, Si, Ge, Sn, Pb$ ) alloys. We perform systematical investigations on  $\Delta E_{total-c/a}$  curves for these alloys under their respective equilibrium cell volumes, which are achieved by their equilibrium lattice constant in the cubic structure. The equilibrium lattice constants in the cubic structure are 5.6 Å, 5.95 Å, 6.01 Å, 5.53 Å, 5.61 Å, 5.87 Å, and 6.01 Å for  $Mn_3Z$  ( $Z = Al, In, Tl, Si, Ge, Sn, Pb$ ) alloys respectively. Their  $\Delta E_{total-c/a}$  curves are shown in Figure 2b. For a clear analogy, the  $\Delta E_{total-c/a}$  curve of  $Mn_3Ga$  is also replotted in Figure 2b, in which one can see that, similar to  $Mn_3Ga$  alloy, there are two local energy minima in the  $\Delta E_{total-c/a}$  curves for all the other  $Mn_3Z$  alloys. One energy minimum is at  $c/a = 1$  (cubic phase), and the other is at  $c/a = 1.35$  (tetragonal phase), except for  $Mn_3Ge$ , where it is at  $c/a = 1.4$ . From Figure 2b, we can observe that when  $Z$  is cognate element, the  $\Delta E_{total}$  of the tetragonal phase at  $c/a = 1.35$  (for  $Mn_3Ge$  at  $c/a = 1.4$ ) decreases gradually with the increase of atomic number. It is also clear that the smaller the atomic number, the smaller the volume of compound. The cubic phase is more stable than the tetragonal phase for the compounds with a small volume, such as  $Mn_3Al$ ,  $Mn_3Ga$ ,  $Mn_3Si$ , and  $Mn_3Ge$ . And the tetragonal phase is more stable in energy for the compounds with bigger atomic number, such as  $Mn_3In$ ,  $Mn_3Tl$ ,  $Mn_3Sn$  and  $Mn_3Pb$ .

The energy barrier between the two local energy minima is crucial to the occurrence of martensitic transformation (or reverse transformation) from the cubic (tetragonal) to tetragonal (cubic) phase. When the energy barrier is higher than the driving forces of phase transformation, the compound is stable in one of two local energy minima, and the martensitic transformation can not occur in the compound. Conversely, when the energy barrier is lower than the driving force of phase transformation,

martensitic transformation may occur in the compound. In addition, from Figure 2b, it can be found that when the Z atom varies from Al to Tl (Si to Pb), the energy barrier exhibits a maximum at  $\text{Mn}_3\text{Ga}$  ( $\text{Mn}_3\text{Sn}$ ) for  $\Delta E_{\text{total}}$ , and the local energy minimum of tetragonal phase changes from positive to negative value with the increasing atomic number.

All the above results imply that the atomic radius of the main group element Z has a great influence on the volume. We can mix different Z elements to obtain  $\text{Mn}_3\text{Z}$  alloys with the different volumes and stable phases. It should be noted that a thermoelastic martensitic transformation from cubic to tetragonal phase may also occur in the  $\text{Mn}_3\text{Z}$  alloys, since the energy barrier can be flexibly regulated by the mixture of different Z elements. So, the  $\text{Mn}_3\text{Z}$  alloys have the potential to be developed into a series of magnetic shape memory alloys originating from thermoelastic martensitic transformation.

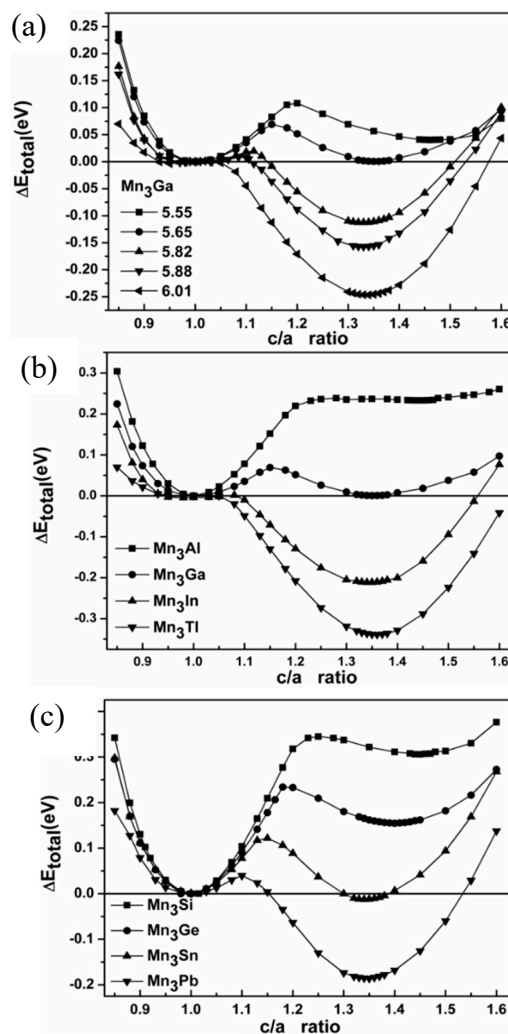


**Figure 2.** (a) Total energy as functions of c/a ratio for  $\text{Mn}_3\text{Ga}$  alloy with different volume ( $V = 17.0 \text{ nm}^3$ ,  $18.0 \text{ nm}^3$ ,  $19.0 \text{ nm}^3$ ,  $20.0 \text{ nm}^3$ ,  $21.0 \text{ nm}^3$ ,  $22.0 \text{ nm}^3$ ). (b) Total energy difference (per formula unit) relative to the cubic phase as a function of c/a for  $\text{Mn}_3\text{Z}$  ( $Z = \text{Al, Ga, In, Tl}$ ) and (c) for  $\text{Mn}_3\text{Z}$  ( $Z = \text{Ge, Sn, Pb}$ ) alloys.

It is well known that with the increase of the distance between the main group Z atom and the nearest neighbor Mn(A) and Mn(C), the hybridization strength of the p-d orbitals between Z and Mn(A/C) atoms is weakened [34]. Before we start to analyze the magnetic properties, we perform an investigation on the change of the relative position of the atoms in  $\text{Mn}_3\text{Z}$  alloys during the tetragonal distortion. As shown in Figure 3a, the distance between Z and Mn(B) and the distance between Mn(A) and Mn(C) along the c axis increase linearly with the increase of the c/a ratio in the process of

tetragonal distortion, while the distance between Z and Mn(B) and the distance between Mn(A) and Mn(C) along the a or b axis decreases linearly with the increase of the c/a ratio. Figure 3b show the changing curve of the distance between two nearest-neighbor atoms with the change of c/a ratio. It is clear that the distance of between two nearest neighbor atoms decreases first, and then increases with the increase of the c/a ratio and get a minimum at  $c/a = 1$ .

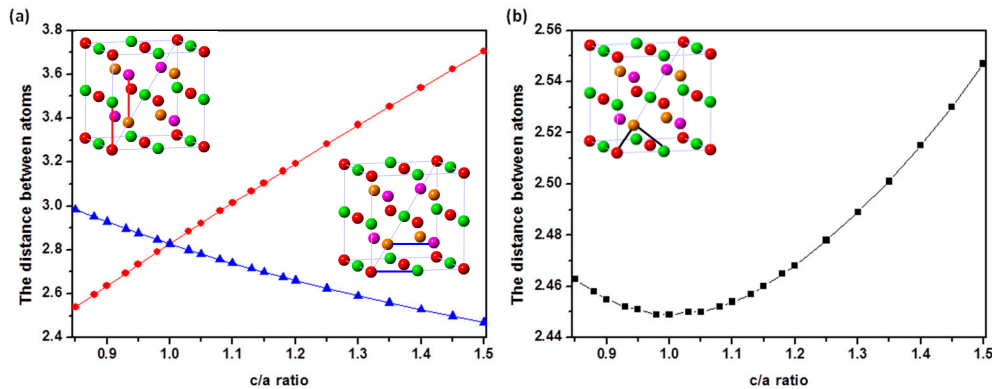


**Figure 3.** The change of interatomic distance in the process of tetragonal distortion for  $Mn_3Ga$  alloy (the lattice constant of cubic structure is  $5.65 \text{ \AA}$ ): (a) The red circle represents the distance between Ga and Mn(B) and the distance between Mn(A) and Mn(C) along c axis. The blue triangle represents the distance between Ga and Mn(B) and the distance between Mn(A) and Mn(C) along a or b axis. (b) The changing curve of the distance between two nearest neighbor atoms with the change of c/a. The thick lines between the atoms in the inset indicate the corresponding interatomic distance).

Next, we will compare and analyze the atomic magnetic moments for the  $Mn_3Ga$  alloy with different volumes, and all the other  $Mn_3Z$  alloys with the equilibrium volume, which are shown in Figures 4 and 5. As we know, with the increase of the lattice constant, the distance between atoms increases, which leads to the weakening of covalent hybridization between atoms. The weakened covalent hybridization will result in an increase of atomic magnetic moments in the Heusler alloys [35,36]. When we compress the lattice along the c-axis ( $c/a < 1$ ), we see that the dependence of the magnetic moment of Mn(A/C) on c/a ratio shows three different tendency ranges with the change of the volume for  $Mn_3Ga$  alloy, as shown in Figure 4a. (1) When the volume is small ( $V = 17 \text{ nm}^3$ ), the magnetic moment of Mn(A/C) atom shows a sharp decrease with the increase of c/a. (2) When the volume is in the range of  $18 \text{ nm}^3 \sim 20 \text{ nm}^3$ , the magnetic moment of Mn(A/C) almost remains constant with the increase of c/a, which indicates that the moment is very stable against the compressive strain along the c-axis. (3) When the volume is higher than  $21 \text{ nm}^3$ , the magnetic moment of Mn(A/C) increases slowly with the increase of c/a.

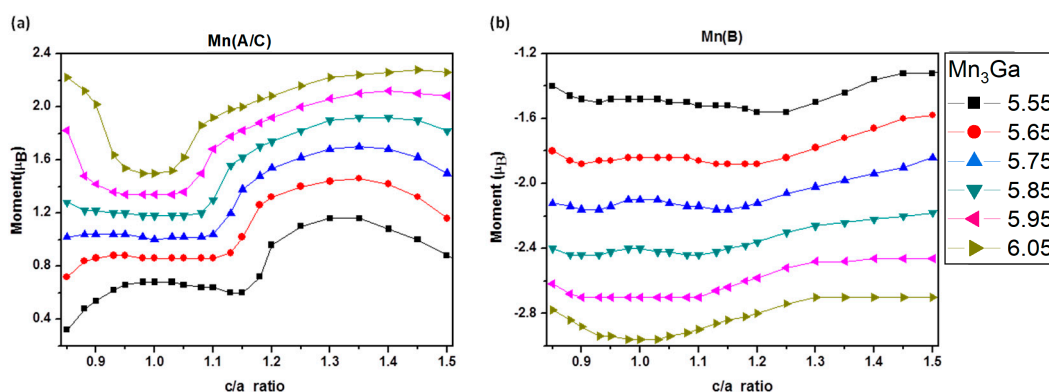


**Figure 4.** The atomic magnetic moments of Mn(A/C) (a) and Mn(B) (b) as functions of c/a ratio for  $Mn_3Ga$  alloy with different lattice constants.

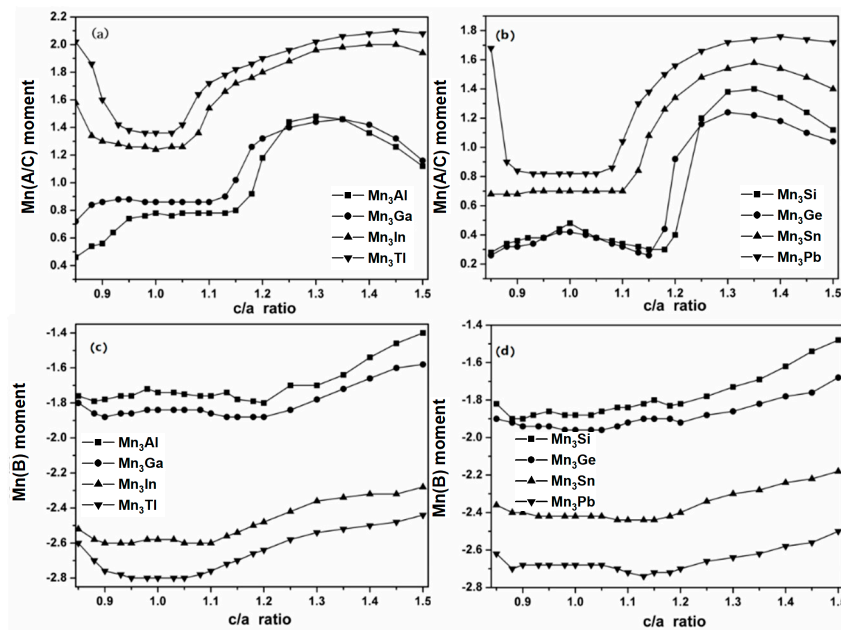


**Figure 5.** The atomic magnetic moments of Mn(A/C) (a,b) and Mn(B) (c,d) as functions of c/a ratio for  $Mn_3Z$  ( $Z = Al, Ga, In, Tl, Si, Ge, Sn, Pb$ ) alloys.

The three different changing trends of the Mn(A/C) moment are due to the change of covalent hybridization between these atoms with the changing tetragonal distortion ratio [37]. There are three kinds of possible covalent hybridizations, i.e., between Ga and Mn(A/C), between Mn(A) and Mn(C) along c axis and between Mn(A/C) and Mn(B), which compete to determine the atomic magnetic moments. When  $c/a < 1$ , with the increase of the c/a ratio, the following occurs: (1) The distance between Ga and Mn(A/C) decreases, which leads to the strengthened p-d orbital covalent hybridization between Ga and Mn(A/C). Thus, the magnetic moment of Mn(A/C) decreases with the increase of c/a ratio. (2) The distance between Mn(A) and Mn(C) along the c axis increases, and the d-d orbital covalent hybridization between them was weakened. So, the magnetic moment of Mn(A/C) increases. (3) The distance between Mn(A/C) and Mn(B), namely, the distance between two nearest neighbor atoms, decreases and the d-d covalent hybridization is strengthened. Thus, the magnetic moments of Mn(A/C) and Mn(B) show a decrease trend. According to the above phenomena, it can be observed that when the volume is small ( $v = 17 \text{ nm}^3$ ), the d-d orbital covalent hybridization between Mn(A) and Mn(C) atoms plays a dominant role to lead to a sharp decrease of the magnetic moment of Mn(A/C) with the increase of c/a. When the volume is greater than  $21 \text{ nm}^3$ , the p-d orbital covalent hybridization between Ga and Mn(A/C) and the d-d orbital covalent hybridization between Mn(A/C) and Mn(B) atoms are the main contributors. As for the cases of  $18\sim 20 \text{ nm}^3$ , which have moderate distances among atoms, the p-d orbital covalent hybridization between Ga and Mn(A/C), the d-d orbital covalent hybridization between Mn(A) and Mn(C) atoms, and the d-d orbital covalent hybridization between Mn(A/C) and Mn(B) atoms counteract each other. Thus, the magnetic moment of Mn(A/C) remains almost unchanged with the increase of c/a.

From Figure 4a, it can also be seen that when  $c/a > 1$ , the moment of Mn(A/C) first increases and then generates a downward trend. We might consider the case of  $c/a < 1$  to understand the situation. Firstly, with the increase of c/a ratio, the distance between Mn(A/C) and Ga (also Mn(B)) increases. So, the p-d (d-d) covalent hybridization decreases and the moment of Mn(A/C) increases. Secondly, the distance between Mn(A) and Mn(C) atoms along c axis increases. Thus, the d-d covalent hybridization was weakened and the magnetic moments of Mn(A/C) increase. Thirdly, with the increase of c/a ratio, the distance between the Mn(A) and Mn(C) along the a or b axis decreases, which leads to the strengthened of d-d covalent hybridization between them and a decrease of the Mn(A/C) moment. So, we can know that the Mn(A/C) magnetic moment increases first, and then decreases with the increase

of  $c/a$ , which may be attributed to the change of covalent hybridization originating from the change of interatomic distance. Furthermore, with the increase of volume, the position of the inflection point to go down gradually shifts to the right. This is because  $Mn_3Ga$  alloy with larger volume needs a larger degree of distortion (a larger  $c/a$  ratio) to make the distance between Mn(A) and Mn(C) along the  $a$  or  $b$  axes sufficiently small to achieve the same strength of d-d orbital covalent hybridization.

The magnetic moment of Mn(B) as a function of  $c/a$  ratio is plotted in Figure 4b for  $Mn_3Ga$  alloys with different volumes. In the process of tetragonal distortion, the distance between Ga and Mn(B) atoms along the  $c$  axis gradually increases, and the p-d orbital covalent hybridization between these atoms gradually weakens, which makes the Mn(B) moment continue to increase. At the same time, the distance between Ga and Mn(B) atom along the  $a$  or  $b$  axis gradually decreases with the increase of  $c/a$  ratio. So, the p-d orbital covalent hybridization between these atoms gradually strengthens and the Mn(B) moment decreases. Thus, we can also understand this changing behavior of the magnetic moment of Mn(B).

Furthermore, from Figure 4b, we can see that the interatomic distance effects on the covalent hybridization counteract each other when  $c/a$  ratio is small for  $Mn_3Ga$  alloys with  $V = 17.0\text{--}21.0\text{ nm}^3$ . And the magnetic moment of Mn(B) moment is essentially unchanged. But when  $c/a$  ratio increases to about 1.2, the p-d orbital covalent hybridization between Ga and Mn(B) atoms along the  $c$  axis plays a major role, and the magnetic moment of Mn(B) has an upward trend. When the volume increases to  $22.0\text{ nm}^3$ , the distance between atoms is quite large, and the covalent hybridization becomes weaker. As  $c/a$  is in the range of 0.85–1, the p-d orbital covalent hybridization between Ga and Mn(B) atoms along the  $a$  or  $c$  axis and the d-d covalent hybridization between Mn(A/C) and Mn(B) are the main contributors, and the magnetic moment of Mn(B) has a downward trend. For the case of  $c/a > 1$ , both the p-d orbital covalent hybridization between Ga and Mn(B) along the  $c$  axis and the d-d covalent hybridization between Mn(A/C) and Mn(B) make the magnetic moment of Mn(B) show an upward trend.

We can see that the magnetic moments of Mn(A/C) and Mn(B) as functions of  $c/a$  ratio are very similar to  $Mn_3Ga$  alloy for all the other  $Mn_3Z$  ( $Z = Al, In, Tl, Si, Ge, Sn, Pb$ ) alloys, as shown in Figure 5. As different main group elements have different atomic radii, the distance between atoms can be tuned by changing the main group element in  $Mn_3Z$  which is similar to that in  $Mn_3Ga$  alloy with different volume.

#### 4. Conclusions

In summary, the structural and magnetic properties of tetragonal Heusler alloys  $Mn_3Z$  ( $Z = Ga, In, Tl, Ge, Sn, Pb$ ) have been systemically investigated by the first-principles calculations. The calculations indicate that the stability of the system is very sensitive to changes of volume. And the volume can be tuned by changing the main group element in  $Mn_3Z$  alloys. The p-d and d-d covalent hybridization play very important roles during the tetragonal distortion, and have great influence on the atomic magnetic moments in  $Mn_3Z$  alloys.

**Author Contributions:** Conceptualization, G.L. and H.Z.; methodology, H.Z.; formal analysis, G.L., H.Z. and W.W.; investigation, H.Z., W.L. and T.L.; writing—original draft preparation, H.Z.

**Funding:** This work was supported by the Program for Leading Talents in Science and Technology Innovation of Chongqing City (No. CSTCKJXCLJRC19) and Natural Science Foundation of Tianjin City (No. 16JCYBJC17200).

**Conflicts of Interest:** The authors declare no conflict of interest.

## References

1. Wollmann, L.; Fecher, G.H.; Chadov, S.; Felser, C. A scheme for spin-selective electron localization in Mn<sub>3</sub>Ga Heusler material. *J. Phys. D Appl. Phys.* **2015**, *48*, 164004. [[CrossRef](#)]
2. Wu, H.K.F.; Sudoh, I.; Xu, R.H.; Si, W.S.; Vaz, C.A.F.; Kim, J.; Vallejo-Fernandez, G.; Hirohata, A. Large exchange bias induced by polycrystalline Mn<sub>3</sub>Ga antiferromagnetic films with controlled layer thickness. *J. Phys. D Appl. Phys.* **2018**, *51*, 215003. [[CrossRef](#)]
3. Wu, F.; Mizukami, S.; Watanabe, D.; Sajitha, E.P.; Naganuma, H.; Oogane, M.; Ando, Y.; Miyazaki, T. Structural and Magnetic Properties of Perpendicular Magnetized MnGa Epitaxial Films. *IEEE Trans. Magn.* **2010**, *46*, 1863–1865. [[CrossRef](#)]
4. Winterlik, J.; Balke, B.; Fecher, G.H.; Felser, C. Structural, electronic, and magnetic properties of tetragonal Mn<sub>3-x</sub>Ga: Experiments and first-principles calculations. *Phys. Rev. B* **2008**, *77*, 054406. [[CrossRef](#)]
5. Feng, W.W.; Thiet, D.V.; Dung, D.D.; Shin, Y.; Cho, S. Substrate-modified ferrimagnetism in MnGa films. *J. Appl. Phys.* **2010**, *108*, 113903. [[CrossRef](#)]
6. Niida, H.; Hori, T.; Onodera, H.; Yamaguchi, Y.; Nakagawa, Y. Magnetization and coercivity of Mn<sub>3-δ</sub>Ga alloys with a D0<sub>22</sub>-type structure. *J. Appl. Phys.* **1996**, *79*, 5946–5948. [[CrossRef](#)]
7. Elm, M.T.; Hara, S. Transport Properties of Hybrids with Ferromagnetic MnAs Nanoclusters and Their Potential for New Magnetoelectronic Devices. *Adv. Mater.* **2014**, *26*, 8079–8095. [[CrossRef](#)]
8. Ma, Q.L.; Kubota, T.; Mizukami, S.; Zhang, X.M.; Naganuma, H.; Oogane, M.; Ando, Y.; Miyazaki, T. Interface tailoring effect on magnetic properties and their utilization in MnGa-based perpendicular magnetic tunnel junctions. *Phys. Rev. B* **2013**, *87*, 184426. [[CrossRef](#)]
9. Winterlik, J.; Chadov, S.; Gupta, A.; Alijani, V.; Gasi, T.; Filsinger, K.; Balke, B.; Fecher, G.H.; Jenkins, C.A.; Casper, F.; et al. Design Scheme of New Tetragonal Heusler Compounds for Spin-Transfer Torque Applications and its Experimental Realization. *Adv. Mater.* **2012**, *24*, 6283–6287. [[CrossRef](#)]
10. Gutierrez-Perez, R.M.; Holguin-Momaca, J.T.; Elizalde-Galindo, J.T.; Espinosa-Magana, F.; Olive-Mendez, S.F. Giant magnetization on Mn<sub>3</sub>Ga ultra-thin films grown by magnetron sputtering on SiO<sub>2</sub>/Si(001). *J. Appl. Phys.* **2015**, *117*, 123902. [[CrossRef](#)]
11. Baltz, V.; Manchon, A.; Tsoi, M.; Moriyama, T.; Ono, T.; Tserkovnyak, Y. Antiferromagnetic spintronics. *Rev. Mod. Phys.* **2018**, *90*, 015005. [[CrossRef](#)]
12. Kurt, H.; Baadji, N.; Rode, K.; Venkatesan, M.; Stamenov, P.; Sanvito, S.; Coey, J.M.D. Magnetic and electronic properties of D0<sub>22</sub>-Mn<sub>3</sub>Ge (001) films. *Appl. Phys. Lett.* **2012**, *101*, 132410. [[CrossRef](#)]
13. Wu, F.; Sajitha, E.P.; Mizukami, S.; Watanabe, D.; Miyazaki, T.; Naganuma, H.; Oogane, M.; Ando, Y. Electrical transport properties of perpendicular magnetized Mn-Ga epitaxial films. *Appl. Phys. Lett.* **2010**, *96*, 042505. [[CrossRef](#)]
14. Sugihara, A.; Suzuki, K.Z.; Miyazaki, T.; Mizukami, S. Magnetic properties of ultrathin tetragonal Heusler D0<sub>22</sub>-Mn<sub>3</sub>Ge perpendicular-magnetized films. *J. Appl. Phys.* **2015**, *117*, 17B511. [[CrossRef](#)]
15. Bai, Z.Q.; Cai, Y.Q.; Shen, L.; Yang, M.; Ko, V.; Han, G.C.; Feng, Y.P. Magnetic and transport properties of Mn<sub>3-x</sub>Ga/MgO/Mn<sub>3-x</sub>Ga magnetic tunnel junctions: A first-principles study. *Appl. Phys. Lett.* **2012**, *100*, 022408. [[CrossRef](#)]
16. Balke, B.; Fecher, G.H.; Winterlik, J.; Felser, C. Mn<sub>3</sub>Ga, a compensated ferrimagnet with high Curie temperature and low magnetic moment for spin torque transfer applications. *Appl. Phys. Lett.* **2007**, *90*, 152504. [[CrossRef](#)]
17. Zhu, L.J.; Nie, S.H.; Meng, K.K.; Pan, D.; Zhao, J.H.; Zheng, H.Z. Multifunctional L1<sub>0</sub>-Mn<sub>1.5</sub>Ga Films with Ultrahigh Coercivity, Giant Perpendicular Magnetocrystalline Anisotropy and Large Magnetic Energy Product. *Adv. Mater.* **2012**, *24*, 4547–4551. [[CrossRef](#)]
18. Zhu, L.J.; Pan, D.; Nie, S.H.; Lu, J.; Zhao, J.H. Tailoring magnetism of multifunctional Mn<sub>x</sub>Ga films with giant perpendicular anisotropy. *Appl. Phys. Lett.* **2013**, *102*, 132403. [[CrossRef](#)]
19. Kurt, H.; Rode, K.; Venkatesan, M.; Stamenov, P.; Coey, J.M.D. High spin polarization in epitaxial films of ferrimagnetic Mn<sub>3</sub>Ga. *Phys. Rev. B* **2011**, *83*, 020405. [[CrossRef](#)]
20. Chadov, S.; Souza, S.W.D.; Wollmann, L.; Kiss, J.; Fecher, G.H.; Felser, C. Chemical disorder as an engineering tool for spin polarization in Mn<sub>3</sub>Ga-based Heusler systems. *Phys. Rev. B* **2015**, *91*, 094203. [[CrossRef](#)]
21. Khmelevskiy, S.; Shick, A.B.; Mohn, P. Prospect for tunneling anisotropic magneto-resistance in ferrimagnets: Spin-orbit coupling effects in Mn<sub>3</sub>Ge and Mn<sub>3</sub>Ga. *Appl. Phys. Lett.* **2016**, *109*, 222402. [[CrossRef](#)]

22. You, Y.R.; Xu, G.Z.; Hu, F.; Gong, Y.Y.; Liu, E.; Peng, G.; Xu, F. Designing magnetic compensated states in tetragonal  $Mn_3Ge$ -based Heusler alloys. *J. Magn. Magn. Mater.* **2017**, *429*, 40–44. [[CrossRef](#)]
23. Jeong, J.; Ferrante, Y.; Faleev, S.V.; Samant, M.G.; Felser, C.; Parkin, S.S.P. Termination layer compensated tunnelling magnetoresistance in ferrimagnetic Heusler compounds with high perpendicular magnetic anisotropy. *Nat. Commun.* **2016**, *7*, 10276. [[CrossRef](#)] [[PubMed](#)]
24. Zhang, D.L.; Yan, B.H.; Wu, S.C.; Kübler, J.; Kreiner, G.; Parkin, S.S.P.; Felser, C. First-principles study of the structural stability of cubic, tetragonal and hexagonal phases in  $Mn_3Z$  ( $Z = Ga, Sn$  and  $Ge$ ) Heusler compounds. *J. Phys. Condens. Matter.* **2013**, *25*, 206006. [[CrossRef](#)] [[PubMed](#)]
25. Yun, W.S.; Cha, G.B.; Kim, I.G.; Rhim, S.H.; Hong, S.C. Strong perpendicular magnetocrystalline anisotropy of bulk and the (001) surface of  $DO_{22} Mn_3Ga$ : A density functional study. *J. Phys. Condens. Matter* **2012**, *24*, 416003. [[CrossRef](#)] [[PubMed](#)]
26. Minakuchi, K.; Umetsu, R.Y.; Ishida, K.; Kainuma, R. Phase equilibria in the Mn-rich portion of Mn–Ga binary system. *J. Alloys Compd.* **2012**, *537*, 332–337. [[CrossRef](#)]
27. Cable, J.W.; Wakabayashi, N.; Radhakrishna, P. Magnetic excitations in the triangular antiferromagnets  $Mn_3Sn$  and  $Mn_3Ge$ . *Phys. Rev. B* **1993**, *48*, 6159–6166. [[CrossRef](#)]
28. Sung, N.H.; Ronning, F.; Thompson, J.D.; Bauer, E.D. Magnetic phase dependence of the anomalous Hall effect in  $Mn_3Sn$  single crystals. *Appl. Phys. Lett.* **2018**, *112*, 132406. [[CrossRef](#)]
29. Segall, M.D.; Lindan, P.J.D.; Probert, M.J.; Pickard, C.J.; Hasnip, P.J.; Clark, S.J.; Payne, M.C. First-principles simulation: Ideas, illustrations and the CASTEP code. *J. Phys. Condens. Matter.* **2002**, *14*, 2717–2744. [[CrossRef](#)]
30. Vosko, S.H.; Wilk, L.; Nusair, M. Accurate spin-dependent electron liquid correlation energies for local spin density calculations: A critical analysis. *Can. J. Phys.* **1980**, *58*, 1200–1211. [[CrossRef](#)]
31. Ye, M.; Kimura, A.; Miura, Y.; Shirai, M.; Cui, Y.T.; Shimada, K.; Namatame, H.; Taniguchi, M.; Ueda, S.; Kobayashi, K.; et al. Role of Electronic Structure in the Martensitic Phase Transition of  $Ni_2Mn_{1+x}Sn_{1-x}$  Studied by Hard-X-Ray Photoelectron Spectroscopy and Ab Initio Calculation. *Phys. Rev. Lett.* **2010**, *104*, 176401. [[CrossRef](#)] [[PubMed](#)]
32. Siewert, M.; Gruner, M.E.; Dannenberg, A.; Chakrabarti, A.; Herper, H.C.; Wuttig, M.; Barman, S.R.; Singh, S.; Al-Zubi, A.; Hickel, T.; et al. Designing shape-memory Heusler alloys from first-principles. *Appl. Phys. Lett.* **2011**, *99*, 191904. [[CrossRef](#)]
33. Felser, C.; Alijani, V.; Winterlik, J.; Chadov, S.; Nayak, A.K. Tetragonal Heusler Compounds for Spintronics. *IEEE Trans. Magn.* **2013**, *49*, 682–685. [[CrossRef](#)]
34. Liu, G.D.; Dai, X.F.; Liu, H.Y.; Chen, J.L.; Li, Y.X.; Xiao, G.; Wu, G.H.  $Mn_2CoZ$  ( $Z = Al, Ga, In, Si, Ge, Sn, Sb$ ) compounds: Structural, electronic, and magnetic properties. *Phys. Rev. B* **2008**, *77*, 014424. [[CrossRef](#)]
35. Li, G.J.; Liu, E.K.; Zhang, H.G.; Zhang, Y.J.; Xu, G.Z.; Luo, H.Z.; Zhang, H.W.; Wang, W.H.; Wu, G.H. Role of covalent hybridization in the martensitic structure and magnetic properties of shape-memory alloys: The case of  $Ni_{50}Mn_{5+x}Ga_{35-x}Cu_{10}$ . *Appl. Phys. Lett.* **2013**, *102*, 062407. [[CrossRef](#)]
36. Zhang, Y.J.; Wang, W.H.; Zhang, H.G.; Liu, E.K.; Ma, R.S.; Wu, G.H. Structure and magnetic properties of  $Fe_2NiZ$  ( $Z = Al, Ga, Si$  and  $Ge$ ) Heusler alloys. *Physica B* **2013**, *420*, 86–89. [[CrossRef](#)]
37. Liu, E.K.; Wang, W.H.; Feng, L.; Zhu, W.; Li, G.J.; Chen, J.L.; Zhang, H.W.; Wu, G.H.; Jiang, C.B.; Xu, H.B.; et al. Stable magnetostructural coupling with tunable magnetoresponsive effects in hexagonal ferromagnets. *Nat. Commun.* **2012**, *3*, 873. [[CrossRef](#)] [[PubMed](#)]

